Investigation of surface-induced alignment of liquid-crystal molecules by optical second-harmonic generation

M. B. Feller, W. Chen,* and Y. R. Shen
Department of Physics, University of California at Berkeley, Berkeley, California 94720
(Received 18 January 1991)

We apply the technique of optical second-harmonic generation to study homogeneously aligned liquid-crystal cells. The surface dipole sensitivity of the technique made it possible to study the monolayer in the absence and presence of a bulk of liquid crystal. By comparing the monolayer orientational distribution functions of three surface treatments (rubbed polymer-coated substrates, rubbed surfactant-coated substrates, and substrates made from oblique evaporation of SiO_x film), we find that two different surface-originated mechanisms are effective in aligning liquid-crystal films. For rubbed polymer samples, it is shown that a short-range molecular interaction is responsible for alignment of the first monolayer, which then aligns the bulk via an epitaxylike interaction. Results on polymers with various structures and compositions and rubbed with a variety of rubbing strengths are presented. For the other surface treatments, the first monolayer is isotropically distributed, indicating that a bulk elastic interaction is responsible for the bulk alignment.

I. INTRODUCTION

Alignment of bulk liquid-crystal (LC) mesophases by properly treated surfaces of substrates is a technique commonly used in the construction of LC devices. Several surface treatments have been successfully employed, but the physical mechanisms affecting the surface-induced bulk alignment are still not well understood. For homogeneous bulk alignment[1] (average molecular orientation along a direction parallel to the surface), the specially treated surfaces often used are rubbed polymer-coated substrates, rubbed surfactant-coated substrates, and substrates covered with an obliquely evaporated SiO_x film. Obviously, as a surface-induced effect, how the first monolayer of LC molecules at the interface is oriented by the surface-molecule interaction is fundamental to our understanding of homogeneous alignment by different substrates.

Berreman[2] first studied the problem by rubbing a glass substrate with diamond paste and creating microgrooves. He calculated the elastic distortion due to the grooves and found that the lowest-energy configuration was for all the molecules to lie along the grooves, creating a uniformly aligned cell along the rubbing direction. Recently, Geary *et al.*,[3] considering alignment of LC films on polymer-coated substrates rubbed with cloth, proposed a different mechanism. Rubbing of the films orients the polymer chains along a preferred direction and the molecular interaction between the LC molecules and the stretched polymer induces the alignment. Both proposed mechanisms lack direct experimental verification of the microscopic pictures they purport.

To study the LC alignment in different cases with different surface treatments, a variety of techniques have been employed. Pretransitional optical birefringence[4–6] and contact angle measurements[7] have been used to deduce the order parameter of LC at various surfaces. Anchoring energy measurements[8] have been carried out to measure the strength of the interaction between the treated surfaces and the LC bulk. All these techniques provide useful information more on the macroscopic properties of an interfacial system. They are not as helpful in probing the LC-substrate interaction at the microscopic level. Researchers have recently used scanning tunneling microscopes (STM) to observe the alignment of LC monolayers on conducting substrates, such as graphite,[9] but the results still need interpretation and most of the systems with practical interest cannot be studied with this technique.

We have demonstrated in recent years that optical second-harmonic generation (SHG) is a powerful method for probing molecules adsorbed at an interface. In particular, it can be used to determine the orientational distribution of a surface monolayer of molecules.[10,11] We have applied the technique to the study of LC monolayers at various interfaces. By monitoring the in-plane symmetry of a LC monolayer evaporated onto a substrate, we can determine whether the monolayer is anisotropically aligned by the treated surface.[10] This then allows us to conclude whether the surface-induced alignment of the LC bulk is of a short-range or long-range nature. For some polymer-coated substrates, we have observed good alignment of the monolayer parallel to the rubbing direction, implying that a molecular epitaxylike interaction is responsible for the bulk alignment. The monolayer alignment is only slightly altered in the presence of a LC bulk. For rubbed surfactant-treated substrates, no detectable anisotropy in the monolayer alignment can be observed, suggesting that the long-range elastic interaction may be responsible for the bulk alignment.

In this paper, we report the details of our SHG studies on the problem of surface-induced homogeneous alignment. A variety of rubbed polymer-coated substrates, rubbed surfactant-coated substrates, and obliquely evaporated SiO_x substrates have been investigated. Polarizing microscope and birefringence measurements were

used to provide supplementary information about the substrates and the samples. In Sec. II we describe the basic theory of how to derive the orientational distribution function from the SHG measurements for a molecular monolayer. The necessary inclusion of some geometrical factors and possible contribution of the LC bulk to the SHG signal is discussed. The SHG results on LC monolayers evaporated onto rubbed and unrubbed substrates coated with several different polymers and surfactants, as well as obliquely evaporated SiO_x are then presented and analyzed in Sec. IV. Finally, in Sec. V, the alignment mechanisms for different surface treatments are discussed. It is shown that the microscopic picture of the alignment derived from our work is consistent with the results of surface anchoring energy measurements.

II. THEORY OF SURFACE SHG

Optical second-harmonic generation as a general surface analytical tool has been described in detail elsewhere.[12] As a second-order nonlinear optical process, it is highly surface specific and allows probing of polar ordering at an interface. With its submonolayer sensitivity, the technique is ideal for studying molecular monolayers at various interfaces. The monolayer characteristics are reflected in the surface nonlinear susceptibility of the monolayer. By measuring the individual components of the nonlinear susceptibility, it is possible to deduce information about the orientation and arrangement of molecules in a monolayer. We are particularly interested in the orientation and alignment of a LC monolayer adsorbed on a solid substrate.

Consider a monolayer of molecules with a second-order polarizability $\alpha^{(2)}$. Assuming that the intermolecular interaction is negligible, as is often the case in the optical response,[13] we can relate the nonlinear susceptibility $\chi^{(2)}$ to the molecular nonlinear polarizability $\alpha^{(2)}$ by

$$\chi^{(2)}_{ijk}=N_s\langle G^{\lambda\mu\nu}_{ijk}\rangle\alpha^{(2)}_{\lambda\mu\nu} \tag{1}$$

where N_s is the surface density of molecules, $G^{\lambda\mu\nu}_{ijk}$ is a transformation matrix connecting the molecular coordinates (ξ,η,ζ) with the substrate coordinates (x,y,z) (see Fig. 1), and the angular brackets denote an average over the molecular orientational distribution. For molecules with a dominant hyperpolarizability element $\alpha^{(2)}_{\xi\xi\xi}$ along the long molecular axis ξ, we can write χ in the simple form

$$\chi^{(2)}_{ijk}=N_s\langle(\hat{\mathbf{i}}\cdot\hat{\boldsymbol{\xi}})(\hat{\mathbf{j}}\cdot\hat{\boldsymbol{\xi}})(\hat{\mathbf{k}}\cdot\hat{\boldsymbol{\xi}})\rangle\alpha^{(2)}_{\xi\xi\xi} . \tag{2}$$

This is the case for many LC molecules, such as the 4-*n*-octyl-4-cyanobiphenyl (8CB) we used in our experiment. Note that Eq. (2) leads to the permutation symmetry

$$\chi^{(2)}_{ijk}=\chi^{(2)}_{jik}=\chi^{(2)}_{kij}=\cdots , \tag{3}$$

which is necessarily satisfied if $\alpha^{(2)}_{\xi\xi\xi}$ is the only dominant element of $\alpha^{(2)}$. Also note that $\chi^{(2)}_{ijk}$ vanishes if the molecules do not form a net polar-oriented layer.

For an isotropic distribution of molecules in the monolayer, there are only two independent nonvanishing components of $\chi^{(2)}$. With a dominating $\alpha^{(2)}_{\xi\xi\xi}$, they are related to the molecular orientation as follows:

$$\begin{aligned}&\chi_{zzz}=N_s\langle\cos^3\theta\rangle\alpha^{(2)}_{\xi\xi\xi} ,\\ &\chi_{zii}=\chi_{izi}=\chi_{iiz}=\tfrac{1}{2}N_s\langle\sin^2\theta\cos\theta\rangle\alpha^{(2)}_{\xi\xi\xi}\end{aligned} \tag{4}$$

where $i,j=x,y$ and θ is the (polar) angle between $\hat{\boldsymbol{\xi}}$ and $\hat{\mathbf{z}}$. If the molecules have a preferred alignment along $\hat{\mathbf{x}}$ in the surface plane, then the resulting C_{1v} symmetry allows six independent, nonvanishing components of χ:

$$\begin{aligned}&\chi^{(2)}_{zzz}=N_s\langle\cos^3\theta\rangle\alpha^{(2)}_{\xi\xi\xi} ,\\ &\chi^{(2)}_{xxx}=-N_s\langle\sin^3\theta\rangle\langle\cos^3\phi\rangle\alpha^{(2)}_{\xi\xi\xi} ,\\ &\chi^{(2)}_{zyy}=\chi^{(2)}_{yzy}=\chi^{(2)}_{yyz}=N_s\langle\cos\theta-\cos^3\theta\rangle\langle1-\cos^2\phi\rangle\alpha^{(2)}_{\xi\xi\xi} ,\\ &\chi^{(2)}_{zxx}=\chi^{(2)}_{xzx}=\chi^{(2)}_{xxz}=N_s\langle\cos\theta-\cos^3\theta\rangle\langle\cos^2\phi\rangle\alpha^{(2)}_{\xi\xi\xi} ,\\ &\chi^{(2)}_{zxz}=\chi^{(2)}_{zzx}=\chi^{(2)}_{xzz}=-N_s\langle\sin\theta-\sin^3\theta\rangle\langle\cos\phi\rangle\alpha^{(2)}_{\xi\xi\xi} ,\\ &\chi^{(2)}_{xyy}=\chi^{(2)}_{yxy}=\chi^{(2)}_{yyx}=-N_s\langle\sin^3\theta\rangle\langle\cos\phi-\cos^3\phi\rangle\alpha^{(2)}_{\xi\xi\xi} ,\end{aligned} \tag{5}$$

where ϕ is the azimuthal angle defined in Fig. 2. Note that we have assumed independent distributions for θ and ϕ.

The above nonvanishing elements of $\chi^{(2)}$ can be measured by surface SHG. We consider here the general case where the monolayer is sandwiched between media 1 and 2. The laser beam is incident from medium 1 and the reflected SH output is detected. Only the interface and medium 2 are assumed to be nonlinear. The SH signal is given by[12]

$$S=\frac{32\pi^3\omega^2\sec^2\theta_1(2\omega)}{c^3[\epsilon_1(2\omega)]^{1/2}\epsilon_1(\omega)}|\chi^{(2)}_{\rm eff}|^2I^2_\omega TA , \tag{6}$$

where I_ω is the intensity of the incident laser beam, T is the laser pulse width, A is the area of the laser spot on the surface, $\epsilon_1(\Omega)$ is the dielectric constant of medium 1 at frequency Ω ($\Omega=2\omega$ or ω), $\theta_1(2\omega)$ is the SH reflection angle, and $\boldsymbol{\chi}^{(2)}_{\rm eff}$ is the effective nonlinear susceptibility. $\boldsymbol{\chi}^{(2)}_{\rm eff}$ has the form

$$\boldsymbol{\chi}^{(2)}_{\rm eff}=[\hat{\mathbf{e}}(2\omega)\cdot\mathbf{L}(2\omega)]\boldsymbol{\chi}^{(2)}:[\mathbf{L}(\omega)\cdot\hat{\mathbf{e}}(\omega)][\mathbf{L}(\omega)\cdot\hat{\mathbf{e}}(\omega)] ,$$

where $\hat{\mathbf{e}}(\Omega)$ are unit polarization vectors for $\Omega=\omega$ or 2ω and $\mathbf{L}(\Omega)$ are appropriate local-field factor tensors, which are defined in Appendixes A and B for the samples we used. The unit polarization vectors for the incident beam and SH beam propagating in the reflected direction, as defined in the laboratory coordinates of Fig. 1, are given by

$$\begin{aligned}&\hat{\mathbf{e}}_i(\omega)=(-\cos\theta_1(\omega),0,\sin\theta_1(\omega)) ,\\ &\hat{\mathbf{e}}_r(2\omega)=(\cos\theta_1(2\omega),0,\sin\theta_1(2\omega))\end{aligned}$$

for p polarization, and

$$\hat{\mathbf{e}}_i(\omega)=\hat{\mathbf{e}}_r(2\omega)=(0,1,0)$$

for s polarization. The total nonlinear susceptibility $\boldsymbol{\chi}^{(2)}$ contains, in general, contributions from both the inter-

faces between medium 1 and medium 2 and the bulk of medium 2.

The signal depends on the same geometry with respect to the beams and on the input and output beam polarizations. Let Φ be the angle between the plane of incidence and the direction of the preferred molecular alignment, i.e., the $\hat{\mathbf{x}}$ axis (see inset in Fig. 1). We then have, for the s-in–s-out polarization combination

$$\chi_{\rm eff}^{(2)}=\chi_{xxx}^{(2)}(\sin^2\Phi)L_y(2\omega)L_y^2(\omega)+3\chi_{xyy}^{(2)}(\cos^2\Phi)(\sin\Phi)L_y(2\omega)L_y^2(\omega)\ .$$

For p in and s out,

$$\chi_{\rm eff}^{(2)}=\chi_{xxx}^{(2)}(\cos^2\Phi)(\sin\Phi)L_y(2\omega)L_x^2(\omega)\cos^2\theta_1(\omega)+\chi_{xyy}^{(2)}(3\sin^3\Phi-2\sin\Phi)L_y(2\omega)L_x^2(\omega)\cos^2\theta_1(\omega)$$
$$+(\chi_{xxz}^{(2)}-\chi_{yyz}^{(2)})(\sin2\Phi)L_y(2\omega)L_x(\omega)L_z(\omega)[-\sin\theta_1(\omega)\cos\theta_1(\omega)]$$
$$+\chi_{xzz}^{(2)}(\sin\Phi)L_y(2\omega)L_z^2(\omega)\sin^2\theta_1(\omega)\ .$$

For s in and p out,

$$\chi_{\rm eff}^{(2)}=\chi_{xyy}^{(2)}(3\cos^3\Phi-2\cos\Phi)L_x(2\omega)L_y^2(\omega)\cos\theta_1(2\omega)+\chi_{xxx}^{(2)}(\sin^2\Phi)(\cos\Phi)L_x(2\omega)L_y^2(\omega)\cos\theta_1(2\omega)$$
$$+\chi_{zxx}^{(2)}(\sin^2\Phi)L_z(2\omega)L_y^2(\omega)\sin\theta_1(2\omega)+\chi_{zyy}^{(2)}(\cos^2\Phi)L_z(2\omega)L_y^2(\omega)\sin\theta_1(2\omega)\ .$$

For p in and p out,

$$\chi_{\rm eff}^{(2)}=\chi_{xxx}^{(2)}(\cos^3\Phi)L_x(2\omega)L_x^2(\omega)\cos\theta_1(2\omega)\cos^2\theta_1(\omega)$$
$$+3\chi_{xyy}^{(2)}(\sin^2\Phi)(\cos\Phi)L_x(2\omega)L_x^2(\omega)\cos\theta_1(2\omega)\cos^2\theta_1(\omega)$$
$$+\chi_{xxz}\cos^2\Phi\{2L_x(2\omega)L_x(\omega)L_z(\omega)[-\cos\theta_1(2\omega)\cos\theta_1(\omega)\sin\theta_1(\omega)]+L_z(2\omega)L_x^2(\omega)\sin\theta_1(2\omega)\cos^2\theta_1(\omega)\}$$
$$+\chi_{yyz}(\sin^2\Phi)\{2L_x(2\omega)L_x(\omega)L_z(\omega)[-\cos\theta_1(2\omega)\cos\theta_1(\omega)\sin\theta_1(\omega)]+L_z(2\omega)L_x^2(\omega)\sin\theta_1(2\omega)\cos^2\theta_1(\omega)\}$$
$$+\chi_{xzz}^{(2)}(\cos\Phi)\{L_x(2\omega)L_z^2(\omega)\cos\theta_1(2\omega)\sin^2\theta_1(\omega)+2L_z(2\omega)L_x(\omega)L_z(\omega)[-\sin\theta_1(2\omega)\sin\theta_1(\omega)\cos\theta_1(\omega)]\}$$
$$+\chi_{zzz}^{(2)}[L_z(2\omega)L_z^2(\omega)\sin\theta_1(2\omega)\sin^2\theta_1(\omega)]\ . \tag{7}$$

In the case where medium 1 is air and medium 2 is glass with little nonlinearity, the contribution from the bulk is negligible.

We can measure SHG as a function of Φ for the four different polarization combinations and, by fitting the data with Eq. (7), we can deduce all the nonvanishing elements of $\chi_{ijk}^{(2)}$. We can then determine, from Eq. (5), $\alpha_{\xi\xi\xi}^{(2)}$ plus five parameters related to molecular orientation. Equation (5) yields

$$\frac{\langle\sin^3\theta\rangle}{\langle\sin\theta\rangle}=\frac{\chi_{xxx}+\chi_{xyy}}{\chi_{xxx}+\chi_{xyy}+\chi_{zxz}}\ ,$$
$$\frac{\langle\cos^3\theta\rangle}{\langle\cos\theta\rangle}=\frac{\chi_{zzz}}{\chi_{zzz}+\chi_{zxx}+\chi_{zyy}}\ . \tag{8}$$

By assuming a Gaussian distribution in θ,

$$f(\theta)=F\exp\left[-\frac{(\theta-\theta_0)^2}{2\sigma^2}\right], \tag{9}$$

where F is a normalization constant, Eq. (8) can be used to determine the average angle θ_0 and the variance σ. For the unrubbed surface, we have $\langle\sin\theta\rangle=\langle\sin^3\theta\rangle=0$, and

$$\frac{\langle\cos^3\theta\rangle}{\langle\cos\theta\rangle}=\frac{1}{1+2\chi_{zyy}/\chi_{zzz}}\ . \tag{10}$$

The distribution in ϕ can be assumed to be a truncated power series,

$$g(\phi)=\sum_{n=0}^{3}d_n\cos(n\phi)\ . \tag{11}$$

The coefficients d_n can then be calculated from the measured $\chi_{ijk}^{(2)}$ using Eq. (5) and knowing $f(\theta)$. The d_2 coefficient describes the surface anisotropy between x and y and is obtained from $\chi_{zxx}/(\chi_{zxx}+\chi_{zyy})$; it is independent of $f(\theta)$. The d_1 and d_3 coefficients describe the asymmetry between x and $-x$. They are deduced from χ_{zxz} and $\chi_{xxx}-3\chi_{xyy}$, respectively.

In our experiment, we are also interested in the orientational distribution of a LC monolayer on a substrate in the presence of the bulk. For this case, medium 1 is the glass substrate and medium 2 is the LC bulk. The bulk contribution to the SHG is no longer zero.[14] In order to be able to deduce $\chi^{(2)}$ for the LC monolayer at the interface from the measurements via Eq. (5), we need to know $\chi_{\rm bulk}^{(2)}$ separately. For LC, $\chi_{\rm bulk}^{(2)}$ can be measured indepen-

dently.[14] The bulk contribution comes mainly from the discontinuity across the interface of the electric quadrupole part resulting from antiparallel pairing of molecules. The total susceptibility used in Eq. (7) is given by[14,15]

$$\chi^{(2)}_{zzz}=\chi^{\text{surface}}_{zzz}-\frac{\chi^{Q}_{zzzz}}{\epsilon(2\omega)\epsilon^2(\omega)}\ ,$$

$$\chi^{(2)}_{zxx}=\chi^{\text{surface}}_{zxx}-\frac{\chi^{Q}_{zzxx}}{\epsilon(2\omega)}\ ,$$

$$\chi^{(2)}_{zyy}=\chi^{\text{surface}}_{zyy}-\frac{\chi^{Q}_{zzyy}}{\epsilon(2\omega)}\ ,$$

with

$$\chi^{Q}_{ijkl}=\tfrac{1}{2}N_B\langle H^{\xi\xi\xi\xi}_{ijkl}\rangle\alpha^{(2)}_{\xi\xi\xi}\xi_0\ , \tag{12}$$

where N_B is the bulk density of LC molecules, ξ_0 is the separation between the chromophores of the antiparallel molecules along $\hat{\xi}$ and H is the transformation matrix. The intrinsic quadrupole contribution from individual LC molecules is usually small in comparison and can be neglected. Equation (16) shows that χ^{Q}_{ijkl} depends on the molecular orientation through $\langle H^{\xi\xi\xi\xi}_{ijkl}\rangle$ and is therefore a function of the bulk orientational order. We consider here a bulk homogeneous alignment along $\hat{\mathbf{x}}$. From Eq. (16), the nonvanishing χ^{Q}_{ijkl} elements for the LC bulk are

$$\begin{aligned}
\chi^{Q}_{zzzz}&=\tfrac{1}{2}N_B\langle\tfrac{3}{8}\sin^4\Theta\rangle\alpha^{(2)}_{\xi\xi\xi}\xi_0\\
&=\tfrac{1}{10}N_B\alpha^{(2)}_{\xi\xi\xi}\xi_0(1-\tfrac{10}{7}\langle P_2\rangle+\tfrac{3}{7}\langle P_4\rangle)\ ,\\
\chi^{Q}_{zzxx}&=\tfrac{1}{2}N_B\langle\tfrac{1}{2}\sin^2\Theta\cos^2\Theta\rangle\alpha^{(2)}_{\xi\xi\xi}\xi_0\\
&=\tfrac{1}{30}N_B\alpha^{(2)}_{\xi\xi\xi}\xi_0[1+\tfrac{5}{7}\langle P_2\rangle-\tfrac{12}{7}\langle P_4\rangle)\ ,\\
\chi^{Q}_{zzyy}&=\tfrac{1}{2}N_B\langle\tfrac{1}{8}\sin^4\Theta\rangle\alpha^{(2)}_{\xi\xi\xi}\xi_0\\
&=\tfrac{1}{30}N_B\alpha^{(2)}_{\xi\xi\xi}\xi_0(1-\tfrac{10}{7}\langle P_2\rangle+\tfrac{3}{7}\langle P_4\rangle)\ ,
\end{aligned} \tag{13}$$

where Θ is the angle between $\hat{\xi}$ and $\hat{\mathbf{x}}$ (the rubbing direction), and $P_2=\frac{1}{2}(3\cos^2\Theta-1)$ and $P_4=\frac{1}{8}(35\cos^4\Theta-30\cos^2\Theta+3)$ are the second and fourth Legendre polynomials, respectively. Both $\langle P_2\rangle$ and $\langle P_4\rangle$ are finite and temperature dependent in the mesophase, jump to zero in the transition to the isotropic phase, and remain zero there. For 8CB, the values of χ^{Q}_{ijkl} have already been measured.[14]

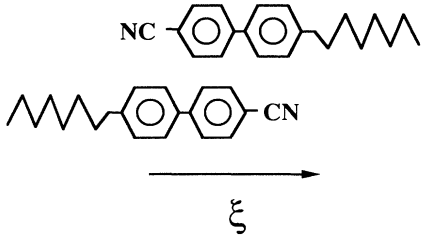

FIG. 2. Schematic depiction of an antiparallel 8CB molecule pair in the bulk.

With the presence of the LC bulk contribution, $\chi^{(2)}_{\text{eff}}$ of Eq. (7) should also experience a jump at the mesomorphic-isotropic transition. The sign of the jump depends on the sign of the bulk contribution, relative to the interfacial contribution from the LC monolayer. In forming quadrupole pairs in the bulk, the LC molecules always have their polar head groups facing each other as pictured in Fig. 2. The surface and bulk contributions should have opposite signs if the surface monolayer is polar oriented with the head groups adsorbed to the substrate. There will also be a change in the local-field factors resulting from the change in the index of refraction of the LC material that occurs at the transition (see Appendix A). This will also affect the value of $\chi^{(2)}_{\text{eff}}$ across the transition.

In the analysis of our SHG data, the local-field factors $L(\Omega)$ in Eq. (7) are important. For spin-coated polymer films on glass substrates, multiple reflections in the polymer films also contribute to the local-field factors. The functional form for the local-field factors for the polymer-coated substrates is presented in Appendix A.

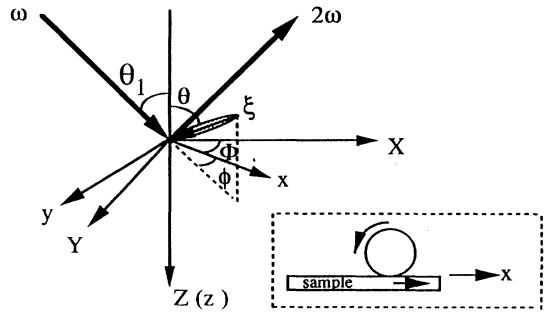

FIG. 1. The long molecular axis ξ in relation to sample coordinates (x,y,z) and laboratory coordinates $(X,Y,Z=z)$. θ and ϕ are polar angle and azimuthal angle of $\hat{\xi}$, respectively, θ_1 is the angle of incidence of the laser beam, and Φ is the sample rotation. The plane of incidence is X-Z. Inset: schematic for the rubbing process. The rubbing direction is along the x axis in the sample frame.

III. EXPERIMENTAL ARRANGEMENT

The experimental setup for measurements of SHG in reflection has been described elsewhere.[12] We used a frequency-doubled, Q-switched, mode-locked, neodymium-doped yttrium aluminum garnet laser (Quantronix 416, Nd:YAG) as the pump. The beam was incident on a sample mounted on a rotating stage. The SH output was detected by a photomultiplier and a gated integrator.

We used the liquid crystal 8CB in our experiment. It exhibits smectic-A (Sm-A) nematic (N), and isotropic (I) phases with transition temperatures $T_{\text{Sm-}A-N}=33.5\,^{\circ}\text{C}$ and $T_{N-I}=40.5\,^{\circ}\text{C}$. Adsorbed 8CB monolayers on substrates were prepared by evaporation, using SHG as an *in situ* probe of the deposition.[16] In all cases, the signal increased quadratically with time and then abruptly saturated, indicating that the molecules adsorbed uniformly onto the substrate until a full monolayer was formed.

Evaporation of 8CB onto all the substrates under investigation exhibited similar temporal behavior.

Polymer films were prepared by spin coating polymer solutions onto fused silica substrates, then baked to eliminate the solvent. The polymers we used are pictured in Fig. 3. The surfactant-coated substrates were prepared through deposition of silane onto the substrates from solution and then polymerized by heating. Methylaminopropyltrimethoxysilane (MAP) was the silane we studied. None of these coated substrates generated a significant SHG signal before deposition of 8CB. The SiO_x-coated substrates were prepared by obliquely evaporating a 200-Å-thick film SiO_x at an angle of 60° with respect to the surface normal.

Rubbing of the substrates was used to induce molecular alignment along the rubbing direction. The rubbing process was carried out by translating a substrate at a constant speed while it is in contact with a rotating wheel of velvet. The rubbing strength can be characterized by the parameter R_s, defined as[17]

$$R_s=\gamma\mathcal{L}\ ,$$

where $\mathcal{L}$ is the total length of cloth in contact with a given point on the substrate and γ is a characteristic coefficient of the interface between the rubbing cloth and the substrate. Generally, γ is a complicated function of the frictional coefficient, the density and length of cloth fibers, the rubbing pressure, etc. For our rubbing geometry, we can write $\mathcal{L}$ as

$$\mathcal{L}=N\ell\left|1\pm\frac{\Omega r}{v}\right|\ ,$$

where N is the number of translations under the wheel, ℓ is the length of cloth in contact with the substrate in one translation, Ω is the angular speed of the rotating wheel, v is the translational velocity of the substrate, and r is the radius of the rubbing wheel. The sign is positive when the directions of motion of the rotating wheel and the substrate are opposite at their point of contact. For our geometry, the sign is negative (see inset of Fig. 1). For our rubbing machine, $\ell=5$ mm, $\Omega/2\pi=68$ rpm, $r=2.5$ cm, and v varied from 0.12 to 0.6 cm/sec. We varied the rubbing strength both by changing the pressure on the polymer-coated substrate, and by changing N or v. Since γ is not a well-defined quantity, we cannot have absolute values for the rubbing strengths, but we can change the relative rubbing strengths by varying $\mathcal{L}$.

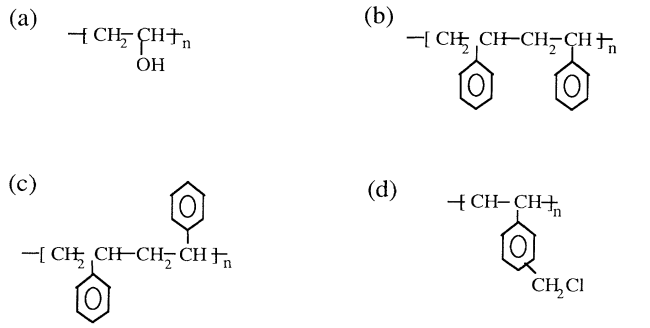

FIG. 3. Molecular structures of the polymers studied (except polyimide). (a) Polyvinyl alcohol (PVA), (b) isotactic polystyrene (PS-*I*), (c) atactic polystyrene (PS-*A*), (d) atactic polyvinylbenzylchloride (PVBC).

The LC cells were prepared for first sandwiching a 130-μm-thick Mylar spacer between two substrates and then filling it by capillary action with 8CB in the isotropic phase. The rubbed substrates induced a homogeneous bulk alignment which was monitored with a polarizing microscope. The anisotropy in the polymer films created by rubbing could be measured by a birefringence measurement using a standard ellipsometry setup.[5]

IV. EXPERIMENTAL RESULTS

A. On polyimide-coated substrates

We monitored the SHG signal from a monolayer of 8CB on rubbed and unrubbed polyimide-coated substrates as a function of the azimuthal orientation of the sample, Φ.[10] An example of the results is presented in Fig. 4. As expected, the signal from the unrubbed substrates is isotropic in Φ. SHG with *s*-in–*s*-out and *p*-in–*s*-out geometries is forbidden by symmetry on an isotropic surface, and therefore generated no detectable signal. On the hard rubbed substrates, however, the signal dependence on Φ is strongly anisotropic and the *s*-in–*s*-out and *p*-in–*s*-out signals are nonzero. The nonzero signal from the *s*-in–*s*-out geometry is evidence that the monolayer orientation is azimuthally anisotropic with at most one mirror plane. We repeated these measurements on polyimide-coated substrates rubbed with a variety of rubbing strengths.

The individual nonvanishing components of the nonlinear susceptibility $\chi^{(2)}$ for the 8CB monolayer in Eq. (5) can be determined from the data in Fig. 4. Specifically, we could obtain $\chi^{(2)}_{xxx}$ from the result at *s*-in–*s*-out and $\chi^{(2)}_{zxx}$ at *s*-in–*p*-out with the sample oriented such that *s* is parallel to the rubbing direction $\hat{\mathbf{x}}$ ($\Phi=90°$). Then, $\chi^{(2)}_{xyy}$, $\chi^{(2)}_{zyy}$, $\chi^{(2)}_{zzz}$, and $\chi^{(2)}_{zxz}$ could all be determined from data points at special geometries according to Eq. (7). Finally, the data from the full angular scan in Fig. 4 could be fit using Eq. (7) to reduce the uncertainty of the values of $\chi^{(2)}_{ijk}$. Our fit of Fig. 4 resulted in a very small standard deviation (less than 1.5×10^{-15} esu). As mentioned in Sec. II, we can use the values obtained for $\chi^{(2)}_{ijk}$ to find approximate distribution functions in θ and ϕ. The results are listed in Table I as the hard rubbing case. The azimuthal distribution function is plotted in Fig. 5.

Measurements of LC monolayers on polyimide-coated substrates rubbed with different rubbing strengths were also carried out and analyzed. The results are summarized in Table I. Sample 1 was unrubbed. Samples 2–5 were rubbed under the same pressure (i.e., identical γ's). Samples 2–4 were passed under the rubbing wheel one, three, and five times, respectively, at a constant velocity of 0.6 cm/sec with the wheel not rotating. Sample 5 was passed under the wheel with the same conditions, except that the wheel was rotating with an angular velocity of 68

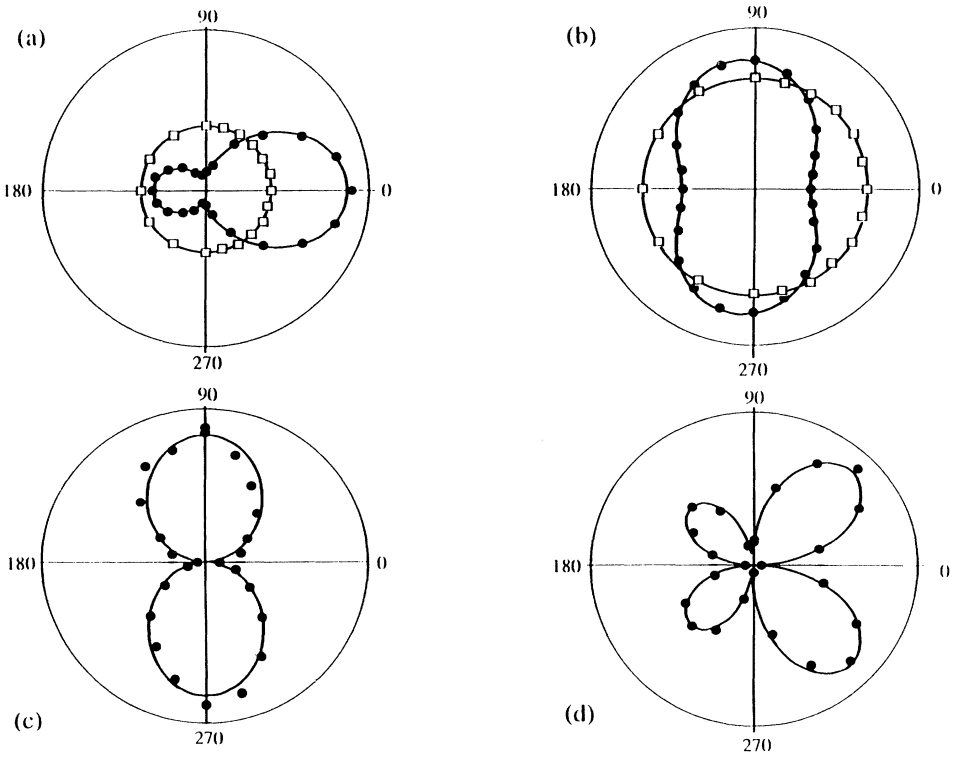

FIG. 4. Square root of second-harmonic signal (arbitary unit) vs sample rotation Φ from an 8CB monolayer on rubbed and unrubbed polyimide-coated substrates. Open squares are data from unrubbed substrates, filled circles are data from substrates rubbed under a hard pressure, and solid lines are the theoretical fits. The input-output polarization combinations are (a) p-in–p-out; (b) s-in–p-out; (c) s-in–s-out; (d) p-in–s-out. The arrow indicates the rubbing direction defined by the arrow in the inset of Fig. 1. Inset: Schematic of preferred orientation of molecular monolayer described by the orientational distribution function.

rpm. Sample 6 was rubbed at a considerably harder pressure. In all cases, we found that $\theta_0 \cong 76°$ and $\sigma = 5°-7°$. While the determination of σ is less certain (10% in standard deviation), the value of θ_0 is accurate to within 2%. For the unrubbed sample, we assume a $\sigma = 5°$ to determine $\theta_0 = 76°$. If we assume a δ-function distribution in θ instead of the Gaussian distribution, we find $\theta_0 = 74°$. The results imply that rubbing of the polymer does not affect the polar orientation of the 8CB molecules.

Figure 5 presents plots of azimuthal orientational distributions of the LC monolayers on the differently rubbed substrates. They show explicitly that rubbing causes the molecule to lie preferentially parallel and antiparallel to the rubbing direction, more antiparallel than parallel (i.e., the chromophores of 8CB molecules tilt more in the direction of the rubbing strokes). The stronger the rubbing strength, the greater is the anisotropy in the monolayer distribution. We also measured the phase of the po-

TABLE I. Results of fits and distribution function parameters for LC monolayers on polyimide-coated substrates that are rubbed at a variety of rubbing strengths. Description of parameters follows: γ is the interfacial parameter; function of rubbing pressure; d_i are coefficients for azimuthal distribution function defined in Eq. (11); θ_0 is the average molecular polar angle for Gaussian distribution defined in Eq. (10); σ is the width of Gaussian distribution for molecular polar angle defined in Eq. (10); and $\Delta\phi$ is the rubbing-induced birefringence in polymer films.

Sample No.	R_s	d_1	d_2	d_3	$\theta_0(\sigma)$	$\Delta\phi$ (mrad)
1	0	0	0	0	76(5)	<0.5
2	1γ	0.019	0.027	0.002	75(7)	<0.5
3	3γ	0.070	0.135	0.015	73(5)	<0.5
4	5γ	0.069	0.148	0.003	76(7)	<0.5
5	10γ	0.099	0.483	0.036	77(5)	1.8
6	hard	0.167	0.762	0.050	77(5)	2.5

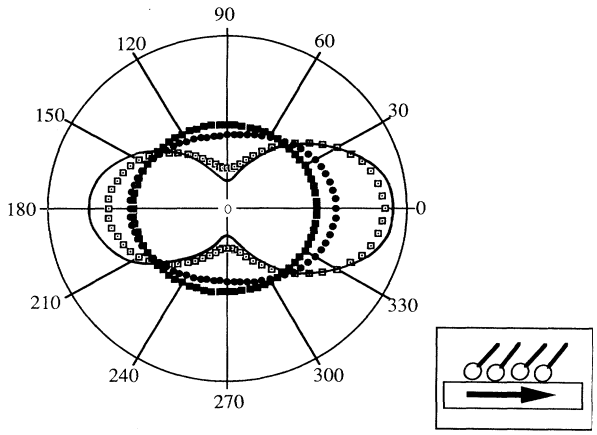

FIG. 5. Azimuthal orientational distribution functions of an 8CB monolayer on polyimide-coated substrates prepared with different rubbing strengths. The squares were for a sample prepared with a rubbing strength $R_s=1\gamma$, the circles were for $R_s=5\gamma$, the squares were for $R_s=10\gamma$. The solid line corresponds to a sample rubbed with $R_s \gg 10\gamma$.

lar monolayer, and found that the head groups pointed toward the substrate for both rubbed and unrubbed polyimide-coated substrates. All the substrates listed in Table I, except the unrubbed one, were effective in inducing a bulk-LC homogeneous alignment in a cell along the rubbing direction.

To see how rubbing affects the polymer films, we measured the birefringence induced in the films by the rubbing with a standard ellipsometry setup.[5] These measurements were limited in their sensitivity by a large background anisotropy in our substrates. We could measure an induced birefringence of $\Delta\phi=0.15$ mrad. Note that the induced birefringence is not a well-defined physical quantity since we do not know over what distance into the bulk of the polymer film the birefringence is distributed, though it has been estimated to be 10–20 nm.[18] However, we used these measurements to qualitatively show that rubbing did reorient the polymer chains and the degree of reorientation increased with the rubbing strength. In our measurements, $R_s=10\gamma$ corresponds to the minimum detectable rubbing-induced birefringence. The LC cells prepared with substrates more lightly rubbed exhibited rather poor homogeneous alignment with stripes of aligned domains. The LC monolayers on such substrates showed no discernible anisotropy in the monolayers. Detailed studies on rubbing-induced birefringence on several polymers have been reported by Geary *et al.* in Ref. 3.

We also carried out SHG measurements on a LC cell made of rubbed polyimide-coated substrates and studied the orientation distribution of the polar-oriented LC monolayer at the LC-substrate interface with the bulk in the isotropic and nematic (ordered) phases. As discussed in Sec. II, we can deduce the values of the surface susceptibility components from the total signal by subtracting out the bulk contribution. The measured SHG as a function of Φ for the four input-output polarization combinations is shown in Fig. 6. In the theoretical fit also shown in Fig. 6, we used Eq. (7) and the results for $\chi^{(2)}_{\text{bulk}}$ from Ref. 12 and obtained $\chi^{(2)}_{ijk}$ for the interfacial LC monolayer from the fit. There exists some uncertainty ($<10\%$) in the values of $\chi^{(2)}_{ijk}$, mainly due to a 10% uncertainty in the index of refraction of LC at the second-harmonic frequency (see Table III). This corresponds to less than a 10% uncertainty in the fitting parameters. The value of χ_{xxz} is less certain ($\leq 20\%$) because it is much smaller. Using the same functional forms for the distributions in θ and ϕ, namely $f(\theta)$ and $g(\phi)$, respectively, given in Sec. II, we found the following results. For $f(\theta)$, we calculated $\theta_0=71°$ with a width of $\sigma=5$. The value of σ is only known within a factor of 2, but θ_0 is known within 2%. The azimuthal distribution function is given by

$$g(\phi)=1+0.06\cos\phi+0.43\cos2\phi-0.001\cos3\phi\ ,$$

which is plotted in Fig. 7 along with the distribution for an 8CB monolayer without the presence of the bulk. The average angles and the distribution function in ϕ for the monolayer in the isotropic cell and for the monolayer in air are very clear, indicating that the bulk has little effect on the surface ordering. Little change in the ordering of the monolayer was observed even when we raised the temperature of the bulk 25 °C above the nematic-isotropic transition, also pointing to the fact that the short-range interaction between the rubbed polymer and the LC molecules is very strong.

We then cooled the LC cell to the nematic phase and repeated the SHG measurements to see if the ordering of the bulk could affect the orientational distribution of the first monolayer. The only experimental geometry that showed significant temperature dependence was the *p*-in–*p*-out geometry which is what we expect since the χ^{Q}_{zzxx} component should have the largest jump across the isotropic-nematic transition according to Eq. (13). For the other experimental geometries, the change of the ordering of the bulk had little effect on the SHG signal, implying that the overall contribution from the bulk is small. The temperature dependence of SHG in the *p*-in–*p*-out geometry is well characterized by taking into account the quadrupole contribution to SHG from the bulk orientational order and the change in the index of refraction of the LC bulk as it goes from the isotropic to the nematic phase. The sign of the jump was correct for the bulk contribution being out of phase with the surface dipole contribution. Thus our results are consistent with the model that the orientation distribution of the first monolayer hardly changes as the bulk goes from the isotropic to the nematic phase.

B. Different polymers

To better understand the nature of the rubbed-polymer–LC interaction, we have looked at LC monolayers on a number of different polymers. The characteristics of the polymers used and the experimental results are summarized in Table II. Polyvinyl alcohol (PVA) produced results most similar to the polyimide. A small, but detectable, rubbing-induced birefringence in

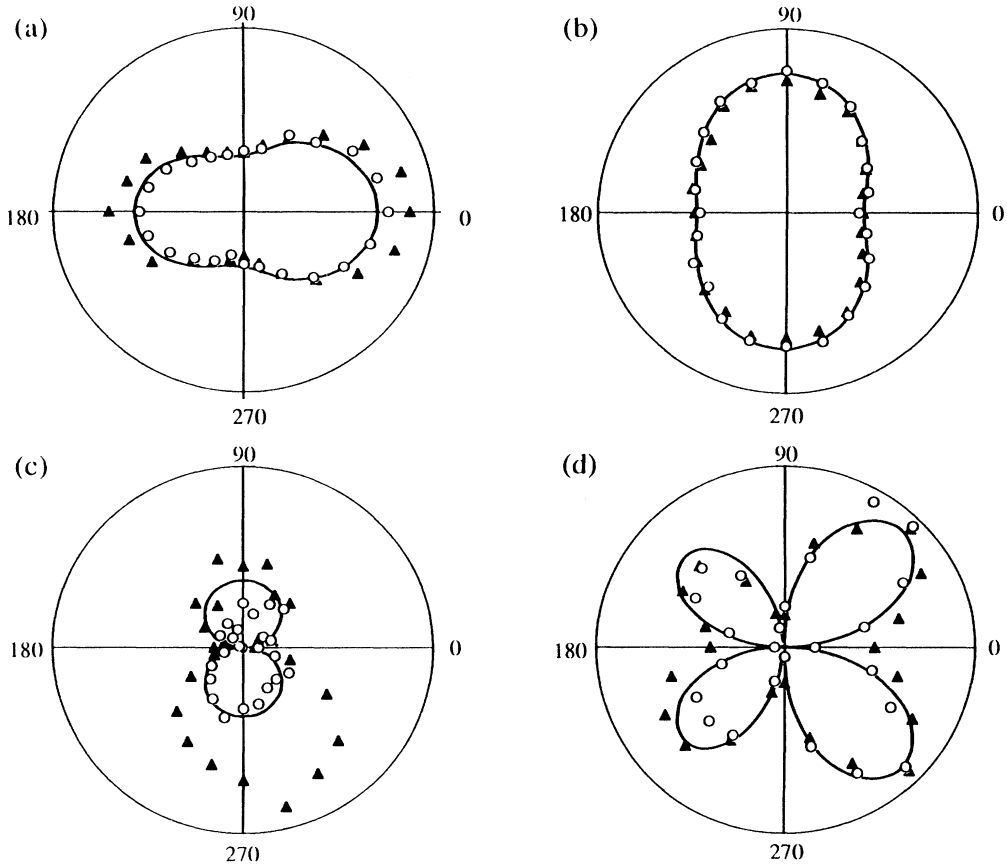

FIG. 6. Second-harmonic output field (arbitrary unit) vs sample rotation Φ from an 8CB cell made with rubbed polyimide-coated substrates. Open circles are data from the cell in the isotropic phase, filled triangles are data from the cell in the nematic phase, and solid lines are the theoretical fits for the isotropic case. The input-output polarization combinations are (a) p-in–p-out; (b) s-in–p-out; (c) s-in–s-out; (d) p-in–s-out.

TABLE II. Physical properties of polymers used.

Polymer coating	Film thickness[a] (Å)	Wt./vol solution (%)	Structure	$\Delta\phi$[b] (mrad)	LC cell alignment[c]	Monolayer alignment[d]
Polyimide (PI)	1200		Crystalline	2.5	↑↑	Yes
Polyvinyl alchohol (PVA)	300	1.5% water	Crystalline	0.5	↑↑	Yes
Isotactic polystyrene (PS-*I*)	500	1.5% toluene	Crystalline	−7	↑↔	No
Atactic polystyrene (PS-*A*)	500	1.5% toluene	Amorphous	−7	Schlieren	No
Polyvinyl benzyl chloride (PVBC)	600	1.5% toluene	Amorphous	−18	Schlieren +↑	Slight

[a]Thickness of spin-coated films is measured by ellipsometry.
[b]Rubbing-induced birefringence in polymer films measured by ellipsometry.
[c]First arrow indicates rubbing direction; second arrow indicates direction of cell alignment relative to rubbing direction. Cell alignment was determined by polarizing microscope.
[d]Results of SHG measurements on distribution of 8CB monolayer evaporated onto treated substrates.

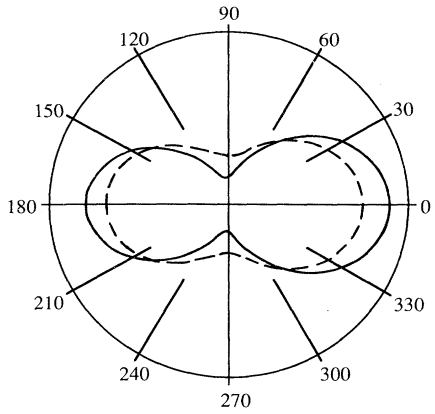

FIG. 7. Azimuthal orientational distribution functions of an 8CB monolayer on rubbed polyimide-coated substrate (solid line), and an 8CB interfacial layer between a rubbed polyimide-coated surface and an 8CB bulk (dashed line).

the PVA film could be measured. LC cells made with PVA-coated substrates had good alignment parallel to the rubbing direction. The LC monolayer alignment on unrubbed and rubbed PVA-coated substrates showed roughly the same orientational distribution as on polyimide. In contrast, polystyrene (PS) has been reported to have a large negative rubbing-induced birefringence, which has been interpreted as a strong ordering of the polymer side groups perpendicular to the rubbing direction.[3,19] We tried substrates coated with atactic polystyrene, where the side groups are randomly oriented about the chain, and found no alignment although the birefringence measurements indicate substantial chain reorientation. With isotactic polystyrene, that has 99% of the side groups on one side of the backbone, however, we found good cell alignment perpendicular to the rubbing direction. For both forms of PS, we were not able to see any significant second-harmonic signal from a monolayer evaporated onto the substrate. This is due to the fact there are no polar sites to which the 8CB head groups could attach to form a polar layer. Polyvinylbenzylchloride (PVBC) is similar to atactic PS, but has methylchloride groups that can act a polar sites. The rubbed PVBC substrates had a very large negative birefringence, yet they led to weak bulk alignment parallel to the rubbing direction, as evidenced by Schlieren defects[20] on a weakly aligned background. The SHG signal from a LC monolayer on a rubbed PVBC-coated substrate was weakly anisotropic, with molecules preferentially aligned along the rubbing direction. In summary, for all these polymers, we found that rubbing leads to a definite reorientation of the polymers and when detectable by SHG, the induced LC monolayer alignment was along the same direction as the bulk alignment.[21]

C. Nonpolymer samples

We have conducted similar SHG measurements on 8CB monolayers evaporated onto MAP-coated substrates.[22] For both rubbed and unrubbed substrates, the SHG signal showed an isotropic dependence on sample orientation rotation about the surface normal for the *s*-in–*p*-out and *p*-in–*p*-out geometries, and vanished for the *p*-in–*s*-out and *s*-in–*s*-out geometries, indicating there is no detectable anisotropy in the distribution of the 8CB monolayer. The results indicate that the LC molecules in the monolayer are not aligned in the surface plane in all cases. From the measured values of $\chi^{(2)}_{zzz}$ and $\chi^{(2)}_{zxx}=\chi^{(2)}_{xzx}$, we found an average polar angle of $\theta_0=70°$ for the 8CB molecules on both rubbed and unrubbed sample substrates assuming a δ-function distribution for θ. We repeated the measurements on a cell made of rubbed MAP-coated substrates.[10] The cell showed good homogeneous alignment along the rubbing direction, as observed under a polarizing microscope. When the cell was in the isotropic phase, the SHG signal was isotropic with respect to the sample orientation about the surface normal, implying that both the bulk and the surface layer are isotropic in the azimuthal plane. When the LC cell was cooled to the nematic phase, we began to see the onset of an anisotropic distribution. The difference from the signal in the isotropic phase is most pronounced in the *p*-in–*p*-out geometry, as it was in the polyimide cell. These results are consistent with the signal expected from an isotropic polar-ordered LC monolayer and a homogeneously aligned LC bulk as described in Eq. (7). The contrast with the polymer-treated substrate is clear—the MAP coating on a substrate has no effect on the LC monolayer alignment in the azimuthal plane, indicating that the surface-LC interaction responsible for the bulk-LC alignment must be macroscopic in nature.

We also studied the molecular distribution of 8CB monolayers on SiO_x substrates. Oblique evaporation of SiO_x leads to sawtoothlike structures forming grooves on the surface.[23] It was thought that LC molecules might lie along the grooves to yield a homogeneously aligned cell. However, since the grooves are much larger than the molecular dimension of a LC molecule, we would no expect a monolayer adsorbed at the surface to be aligned. To determine the orientational distribution of a monolayer on such substrates, we did the following experiments. First, it was determined that an 8CB cell constructed with these substrates exhibited very good bulk homogeneous alignment. Second, we measured SHG from a clean obliquely evaporated SiO_x substrate as a function of the sample rotation, and observed an anisotropic dependence. This is shown in Fig. 8(a). The observed anisotropy is a geometrical effect. The grooved surface causes the local input and output polarizations as well as the local angle of incidence to vary with the sample rotation about the surface normal. They can be taken into account in the calculation of the geometrical local-field factors. In Appendix B, we present a model for the sawtooth structure and calculate SHG from the surface. The observed anisotropy can be qualitatively reproduced [see Fig. 8(c)]. Third, we heated the sample to 250 °C in air, oxidizing SiO_x into SiO_2, which showed negligible SHG contribution. We then deposited an 8CB monolayer onto the SiO_2 grooved substrate by either evaporation or spreading with a solvent. The SHG signal from

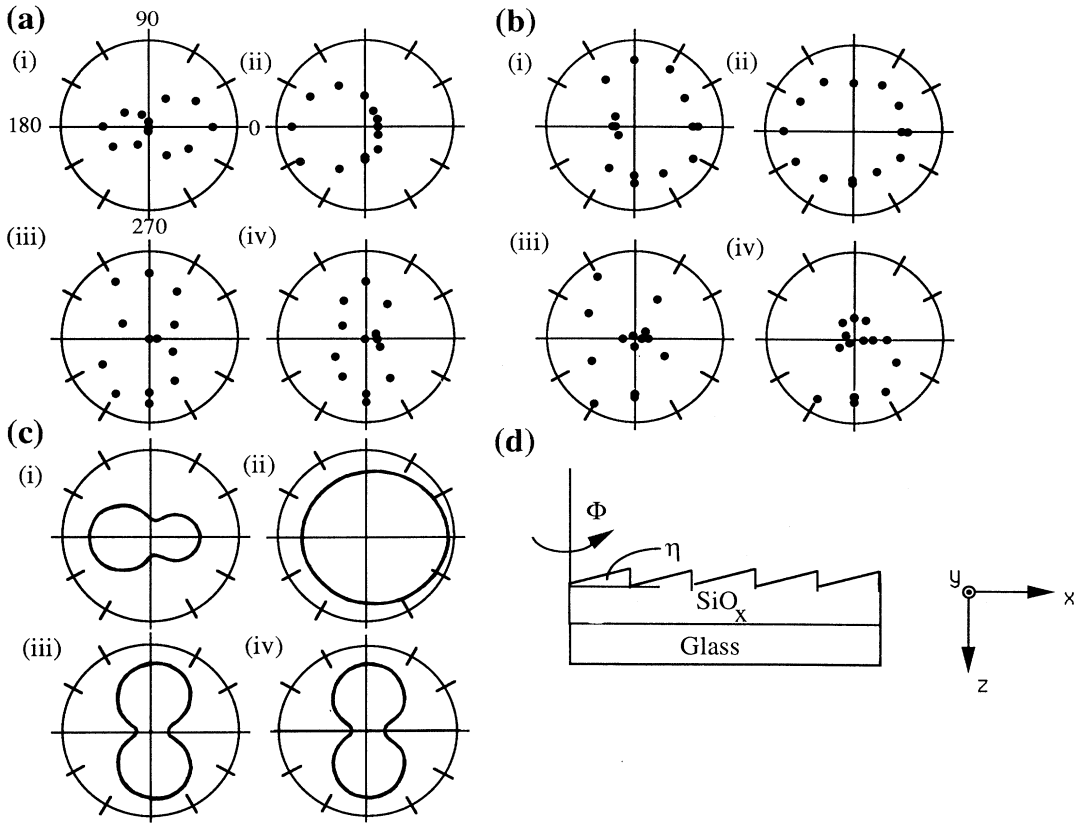

FIG. 8. (a) Second-harmonic output field (arbitrary unit) vs sample rotation Φ from a bare obliquely evaporated SiO_x substrate. (b) Second-harmonic output field (arbitrary unit) vs sample rotation Φ from an 8CB monolayer on an obliquely evaporated SiO_2 substrate. (c) Results of model calculations for output second-harmonic field (arbitrary unit) vs sample rotation Φ from a wedged substrate. For all three sets of plots, the input-output polarization combinations are (i) p-in–p-out; (ii) s-in–p-out; (iii) s-in–s-out; (iv) p-in–s-out. (d) Schematic of SiO_x sample.

the sample now appeared to have an azimuthal anisotropy similar to that observed on the clean SiO_x substrate [see Fig. 8(b)]. Note that the anisotropy observed here is markedly different from the one expected for a monolayer preferentially aligned along the direction of the grooves (see Fig. 2). For the former, the anisotropic distribution has a mirror plane perpendicular to the grooving direction, but for the latter, the mirror plane is parallel to the grooves. This indicates that the observed anisotropy is still a geometrical effect. By analyzing our data as from a locally isotropic monolayer on a sawtooth surface, we were able to account for the observed anisotropy in the SHG signal. Thus the LC bulk alignment mechanism in this case must come from the long-range surface-LC interaction affected by the grooves.

The anisotropy in the surface geometry limits our ability to quantitatively measure anisotropy in the orientational distribution of a LC monolayer on the grooved surface. This is particularly true for the evaporated SiO_x surfaces as they are poorly defined in reality.

V. DISCUSSION

Two models are commonly used to describe surface-induced homogeneous alignment of LC cells. The groove model,[2] applicable to obliquely evaporated SiO_x substrates, proposes that with the LC molecules aligned along the groove direction, the bulk elastic energy from the long-range interaction is minimized. The molecular epitaxylike model applies to rubbed polymer surfaces.[3] It suggests that rubbing reorients the polymer chains at the surface, similar to cold drawing of bulk polymer samples. The adsorbed LC monolayer is then preferentially aligned by interacting directly with the oriented polymer surface and this alignment is extended into the bulk, analogous to epitaxial growth. To data, the physics of surface-induced alignment in liquid crystals has been mostly studied through measurements of the surface anchoring energy,[8] which is a macroscopic interfacial parameter that describes the interaction of a LC bulk with a surface. For $|\theta-\theta_0| \ll 1$, the interfacial free energy is usually written in the form[24]

$$U_{\text{interfacial}} = \tfrac{1}{2} A (\theta-\theta_0)^2 ,$$

where θ is the angle of the director at the interface, θ_0 is the preferred direction, and A is the anchoring strength, or the anchoring energy. However, the microscopic picture of this surface anchoring is not very clear. Here, we try to relate our SHG measurements, which are at the microscopic level, to the surface anchoring energy measurements.[8]

Generally, two surface anchoring energies are used to describe homogeneously aligned LC films. Polar anchoring refers to resistance to distortion of the director from an easy axis in the polar angle, and azimuthal anchoring to distortion in the azimuthal angle. The two anchoring energies have been measured for rubbed surfactant-coated substrates,[25–27] obliquely evaporated SiO_x substrates,[28,29] and rubbed polymer-coated substrates.[8,30] For rubbed MAP substrates, the measured azimuthal anchoring energy is 5×10^{-3} erg/cm^2, and the measured values for the polar anchoring energy range from 5×10^{-3} to 5×10^{-2} erg/cm^2. The azimuthal anchoring energy for SiO_x substrates is on the order of 1×10^{-3} erg/cm^2 while the polar anchoring energy is of 1×10^{-2} erg/cm^2. In these cases, the anchoring energies are sensitive functions of temperature near the isotropic-nematic phase transition. Both the polar and azimuthal anchoring energies have been measured for rubbed polyimide as a function of rubbing strength. The polar anchoring energy is 1 erg/cm^2 is independent of the rubbing strength. The azimuthal anchoring energy is $5-14\times10^{-3}$ erg/cm^2, and is strongly dependent on rubbing strength. The polar anchoring energy of rubbed PVA is 1.5 erg/cm^2, and has little temperature dependence. The temperature dependence of the azimuthal anchoring energy for polymer-coated substrates has not yet been measured. We notice that the anchoring energies associated with the rubbed polymers are two to three orders of magnitude larger than the other surface treatments for the polar case, and up to one order of magnitude larger for azimuthal case. This implies that the alignment force based on the short-range interaction between the rubbed polymers and the first layer of LC is significantly stronger than the one based on minimization of the elastic energy of the bulk.

Our SHG results, which can provide microscopic pictures for the two different alignment mechanisms, are consistent with these anchoring energy results. For the rubbed polymers, our experiments clearly demonstrate the existence of a strong molecular interaction between the rubbed polymers and the first layer of LC molecules. The birefringence measurements imply that the rubbing process leads to a reorientation of polymer chains on the surfaces of all the polymers we have studied.[3] The SHG results show that the stronger rubbing strengths yield better alignment of the monolayer, directly relating the polymer chain reorientation to the LC monolayer alignment. This is a clear indication that a short-range molecular interaction exists between the reoriented polymer and the liquid-crystal molecules. This interaction is quite strong as evidence by the preservation of the monolayer alignment in the presence of an isotropic bulk heated well above the transition temperature. The homogeneous bulk alignment is obviously an extension of the surface alignment via the molecular epitaxylike interaction. The alignment of the LC bulk perpendicular to the rubbing direction for the isotactic PS-coated substrates provides further evidence to this mechanism. Crystalline polymers seem necessary for the LC alignment, further supporting the epitaxial picture. Crystallinity here means regular arrangement of the polymer chains including the side groups. Isotactic PS has a high degree of crystallinity, whereas atactic PS is not. Both atactic and isotactic PS showed the same rubbing-induced negative birefringence but only the isotactic PS led to bulk alignment. The PVBC we used was atactic and exhibited rubbing-induced negative birefringence. No LC alignment perpendicular to the rubbing direction could be observed with PVBC-coated substrates. (A weak interaction between the oriented polymer backbone and the LC molecules might be responsible for the observed weak alignment of the LC monolayer parallel to the rubbing direction.)

For the obliquely evaporated SiO_x substrates, our results suggest that the groove mechanism for the bulk-LC alignment is dominant. In a LC monolayer, the LC-LC interaction is negligible compared to the LC-substrate interaction. Hence a monolayer of liquid crystal should not show any preferred alignment in the absence of surface-induced ordering. This is the case with the obliquely evaporated SiO_x substrates as our measurements show that the LC monolayer is isotropically distributed. Application of the "groove" model to silanes is somewhat controversial since there are conflicting reports on whether rubbing actually creates grooves on the silane-coated substrate. Our finding of no azimuthal anisotropy in the LC monolayer on such a substrate suggests that the short-range interaction is not responsible for the homogeneous bulk alignment. The above descriptions of the LC-substrate interactions are also consistent with the orientational wetting behavior of the various substrates.[4] Ellipsometry measurements show that the orientational order of a bulk nematic LC is greatly reduced near the surface of grooved substrates, implying that, locally, the LC molecules favor an isotropic alignment.[31] On the other hand, on the rubbed polymers, orientational order is clearly enhanced near the surface.

To connect our pictures with the anchoring energy results, we first realize that the latter are not a direct measure of the interaction between the LC monolayer and the substrate. We expect that, for the rubbed polymer case, the interaction energy $U_{\text{LC-substrate}}$ per molecule is significantly larger than $U_{\text{LC-LC}}$ per molecule. If the anchoring energy were equivalent to $U_{\text{LC-substrate}}$, then for a measured polar anchoring energy of ~1 erg/cm^2, for example, we would have $U_{\text{LC-substrate}}$ 3×10^{-15} erg/molecule. This is less than $U_{\text{LC-LC}}\sim kT\sim4\times10^{-14}$ erg/molecule, contrary to what one expects.

The anchoring energies are actually macroscopic quantities. They are related, by definition, to the orientation order parameter near a surface. A smaller order parameter results in a smaller anchoring energy. For example, a weakening of the anchoring energy on evaporated SiO_x and rubbed surfactant-coated substrates as the LC approaches the isotropic-nematic phase transition is a manifestation of a reduction of the order parameter near the surface.[29] For the polymer-coated substrates, the large surface-induced order parameter is the source of the measured high anchoring energy.

We can, however, establish a clear connection between the anisotropy in the surface LC monolayer alignment and the anchoring energies. We know from our measurements that rubbing on the polymer surface induces an anisotropic distribution in the adsorbed LC monolayer.

The harder we rub, the more azimuthally anisotropic is the distribution while the polar orientation of the monolayer remains unchanged. These results are consistent with the surface anchoring energy measurements on rubbed polyimide:[30] the azimuthal anchoring energy was found to be linear in the rubbing strength while the polar anchoring energy was independent of the rubbing strength. This is expected since the polar angle distribution of LC molecules at the surface is determined by the bonding between the molecule and the surface and therefore is not likely to be influenced by rubbing. On obliquely SiO_x and rubbed MAP-coated substrates, our SHG measurements indicate that the surface LC monolayer is isotropically distributed in the plane. The azimuthal anchoring energy on these substrates was found to be appreciably smaller than on rubbed polyimide. The finite anchoring energy in these cases, however, shows again that it is not a direct measure of the LC-substrate interaction but is affected by interaction throughout the interfacial regime. In fact, the adsorbed LC monolayer should be considered as part of the substrate. We can then describe the interfacial LC-substrate interaction as occurring between the adsorbed LC monolayer and the LC bulk. Knowing the distribution of LC molecules on the surface is obviously the first step to understanding this interaction on a microscopic level. By combining the SHG results with the results from ellipsometry measurements, which can tell us the interfacial profile of the order parameter, we could expect to find a clearer picture for the surface-induced LC alignment both microscopically and macroscopically.

VI. CONCLUSION

We have demonstrated that optical SHG can be used to determine quantitatively the orientational distribution of a monolayer of molecules adsorbed on a substrate. Application of the technique to liquid-crystal monolayers on various substrates allows us to study how a surface can induce a bulk-LC alignment. It was shown that a rubbed polymer surface can effectively align the LC monolayer along the rubbing direction, and then via the epitaxylike LC-LC interaction, the alignment is extended to the bulk. On obliquely evaporated SiO_x and rubbed surfactant-coated surfaces, the LC monolayer was found to orient isotropically in the azimuthal plane. This indicates that the surface-induced homogeneous bulk alignment arises from minimization of the elastic interaction in the interfacial region constrained by the grooves on the boundary surface. Our results can be linked with the known values of anchoring energies on these surfaces, although the latter are more ill-defined macroscopic quantities.

ACKNOWLEDGMENTS

This work was supported by National Science Foundation–Solid State Chemistry Grant No. DMR8717137. M.F. acknowledges support from AT&T Bell Laboratories. We would like to thank K. H. Yang of IBM for providing the polyimide solution.

APPENDIX A: LOCAL-FIELD CORRECTIONS FOR POLYIMIDE-COATED SUBSTRATES

In Eq. (6) of the text, we presented a general expression for the SH signal generated by an interface whose nonlinear susceptibility is described by $\chi^{(2)}_{\rm eff}$. In order to determine accurately the value of $\chi^{(2)}_{\rm eff}$, we must calculate the macroscopic local-field corrections (or Fresnel coefficients) to the incident laser fields and to the SH field generated at the interface. The local-field factors, $L(\Omega)$ (where $\Omega=\omega$ for the incident field and $\Omega=2\omega$ for the SH field), take into account the reflection, refraction, and enhancement of the fields due to the presence of the interface. In this appendix, we will outline the derivation of the local-field factors used to analyze our SH signal from polymer-coated substrates. By taking into account the multiple reflections due to the finite thickness of the polymer films, we improve the accuracy of our local-field factors by approximately 15%. Separate expressions must be derived for the case when the monolayer of liquid crystals is in air and when it is in contact with the LC medium.

A detailed derivation of the local-field factors for the general case of a polarization sheet sandwiched between two infinite bulk media is presented in Ref. 12. It shows that the input local-field factors relating the input field $\mathbf{E}_{\rm laser}(\omega)$ in medium 1 to the corresponding field components in the polarization sheet $\mathbf{E}_{\rm source}(\omega)$ are given by

$$
\begin{aligned}
L_{xx}(\omega)&=\left.\frac{E_{\rm source}}{E_{\rm laser}}\right|_x=\frac{2n_1(\omega)\cos\theta_2}{n_2(\omega)\cos\theta_1+n_1(\omega)\cos\theta_2}\ ,\\
L_{yy}(\omega)&=\left.\frac{E_{\rm source}}{E_{\rm laser}}\right|_y=\frac{2n_1(\omega)\cos\theta_1}{n_1(\omega)\cos\theta_1+n_2(\omega)\cos\theta_2}\ ,\\
L_{zz}(\omega)&=\left.\frac{E_{\rm source}}{E_{\rm laser}}\right|_z\\
&=\frac{2n_1^2(\omega)n_2(\omega)\cos\theta_1}{n_m^2(\omega)[n_2(\omega)\cos\theta_1+n_1(\omega)\cos\theta_2]}\ ,
\end{aligned}
\tag{A1}
$$

where n_1, n_2, and n_m are indices of refraction of the media 1 and 2 and the polarization sheet, respectively.

The output local-field factors are defined in the following way. The field radiated from a polarization sheet $\mathbf{P}^s(2\omega)$, is[12]

$$
E(2\omega)=\frac{4\pi i\omega\sec\theta_1(2\omega)}{c[\epsilon_1(2\omega)]^{1/2}}[\hat{\mathbf{e}}(2\omega)\cdot\mathbf{L}(2\omega)\cdot\mathbf{P}^s(2\omega)]\ , \tag{A2}
$$

where all the geometric factors resulting from the reflection and refraction at the interface are contained in $\mathbf{L}(2\omega)$. The wave vector of the radiation at 2ω has components along both the positive and negative z axes. Their directions are determined by the constraint imposed by conservation of the tangential component of the wave vectors. In the reflection direction (along the negative z axis), the output local-field factors $[L_{ii}(2\omega)=L_{ii}^R(2\omega)]$ have the exact same form as that of the input local-field factors of Eq. (A1), using the values of the indices of refraction at 2ω. In the transmitted direction (along the positive z axis), the output local-field factors

$[L_{ii}(2\omega)=L_{ii}^{T}(2\omega)]$ also have the same form as Eq. (A1) if we exchange subscripts 1 and 2 and use the values of the indices of refraction at 2ω.

We now want to derive the expressions for the local-field factors for the thin-film system that represents the polymer-coated substrates. The two geometries we must consider for the polymer-coated substrates are pictured in Fig. 9.

The input local-field factors for both systems are straightforward. For the monolayer case pictured in Fig. 9(a), we can apply the rule of continuity of E_x, E_y, and D_z across the interface to show that the input field in the polymer film is given by

$$L_{xx}^{a}(\omega)\equiv\frac{E_x(\omega)|_{\text{source}}}{E_x(\omega)|_{\text{laser}}}=1-r_p\ ,$$
$$L_{yy}^{a}(\omega)\equiv\frac{E_y(\omega)|_{\text{source}}}{E_y(\omega)|_{\text{laser}}}=1+r_s\ , \tag{A3}$$
$$L_{zz}^{a}(\omega)\equiv\frac{E_z(\omega)|_{\text{source}}}{E_z(\omega)|_{\text{laser}}}=(1+r_p)\left[\frac{n_2}{n_m}\right]^2\ ,$$

where $r_{s,p}$ denotes the field reflection coefficient of the s- or p-polarized light reflected from the interface. We have

$$r_k=\frac{r_{12k}+r_{23k}e^{2i\beta}}{1+r_{12k}r_{23k}e^{2i\beta}}\ , \tag{A4}$$

where medium 1 is air, medium 2 is polymer, medium 3 is substrate, $k=s$ or p polarization, r_{12} and r_{23} are linear Fresnel reflection factors at interface 1,2 and interface 2,3, respectively, and $\beta=(2\pi/\lambda_0)n_2h\cos\theta_2(\omega)$, with λ_0 being the laser wavelength in air, h the thickness of the polymer film, and $\theta_2(\omega)$ the transmission angle in the polymer film as determined by the continuity of the tangential component of the wave vector. The values we used for the indices of refraction are listed in Table III. Note, for h going to zero, these equations are equivalent to Eq. (A1).

The input local-field factors for the cell case, as pictured in Fig. 9(b) must take into account the transmission through the air-substrate interface and transmission through the polymer film. We find

$$L_{xx}^{b}(\omega)=\left.\frac{E_{\text{source}}}{E_{\text{laser}}}\right|_x=t_pt_{13p}\ ,$$
$$L_{yy}^{(b)}(\omega)=\left.\frac{E_{\text{source}}}{E_{\text{laser}}}\right|_y=t_st_{13s}\ , \tag{A5}$$
$$L_{zz}^{(b)}(\omega)=\left|\frac{E_{\text{source}}}{E_{\text{laser}}}\right|_z=t_pt_{13p}\left[\frac{n_4}{n_m}\right]^2\ ,$$

where $t_k=t_{32k}t_{24k}/(1+r_{32k}r_{24k}e^{2i\beta})$, media 1, 2, and 3 are air, polymer, and substrate, respectively, medium 4 corresponds to liquid crystal bulk, and β is defined earlier. If the LC is in the nematic phase, the uniaxial property of the LC needs to be considered in calculating $t_{s,p}$.

The local-field factors for the second-harmonic output in the geometries of Fig. 9(a) can also be found. We will present the derivation for the s component of the monolayer case, i.e., $L_{yy}(2\omega)$, in detail; the derivation of $L_{xx}(2\omega)$ and $L_{zz}(2\omega)$ is similar [see Fig. 9(a)]. Two SH fields radiate from the LC monolayer, one in the reflected direction ($-z$ direction) and one in the transmitted direction ($+z$ direction). The field radiated in the $+z$ direction will reflect off the polymer-substrate interface, leading to an additional contribution to the output field. The total contribution to the field radiating into medium 1 is

$$E_{\text{detected},s}=E_{s_1}+r_s'E_{s_2}\ . \tag{A6}$$

According to Eq. (A2), the fields are written as

$$E_{s_1}(2\omega)=\frac{4\pi i\omega\sec\theta_1(2\omega)}{c[\epsilon_1(2\omega)]^{1/2}}L_{yy}^{R}(2\omega)P^{s}y\ ,$$
$$E_{s_2}(2\omega)=\frac{4\pi i\omega\sec\theta_2(2\omega)}{c[\epsilon_2(2\omega)]^{1/2}}L_{yy}^{T}(2\omega)P^{s}y\ ,$$

where $L_{yy}^{R}(2\omega)$ and $L_{yy}^{T}(2\omega)$ are the output local-field factors for the air-polymer interface and have the same form as Eq. (A1) and $r_s'=r_{23k}t_{21k}e^{2i\beta}/(1+r_{12k}r_{23k}e^{2i\beta})$ is the field reflection coefficient for the radiation back into medium 1. Using the general definition for $\mathbf{L}(2\omega)$ as given in Eq. (A2), we have, for the y component of $\mathbf{L}$ of the thin-film system,

$$L_{yy}(2\omega)=L_{yy}^{R}(2\omega)+\left[\frac{\epsilon_1(2\omega)}{\epsilon_2(2\omega)}\right]^{1/2}\frac{\sec\theta_2(2\omega)}{\sec\theta_1(2\omega)}L_{yy}^{T}(2\omega)r_s'\ . \tag{A7}$$

With the known expressions of $L_{yy}^{R}(2\omega)$ and $L_{yy}^{T}(2\omega)$, we can rearrange Eq. (A7) to obtain

$$L_{yy}(2\omega)=1+r_s\ ,$$

where r_s is defined in Eq. (A4). Thus the ouput local-field factor for the thin-film polymer sample has the same form as the input local-field factor with the indices of refraction at 2ω, as in the case of a single interface. After

TABLE III. Indices of refraction used to calculate local-field corrections.

Medium	$n(\omega)$	$n(2\omega)$
Air	1.00	1.00
Fused silica substrate	1.46	1.50
Polyimide	1.60[a]	$1.80+0.03i$[a]
8CB bulk—isotropic	1.56[b]	$1.4+0.2i$[a]
8CB bulk—nematic extraordinary	1.65[b]	$1.36+0.41i$[c]
8CB bulk—nematic ordinary	1.52[b]	$1.45+0.10i$[c]
8CB—monolayer (ϵ_m)	1.00	1.00

[a]Reflectivity measurements conducted by authors. Uncertainty in measurements is ±0.02.

[b]D. A. Dunmar, M. R. Manterfield, W. H. Miller, and J. K. Dunleavy, Mol. Cryst. Liq. Cryst. **45**, 127 (1978).

[c]Reflectivity measurements conducted by authors. Uncertainty in measurements is 10%.

carefully calculating the p-polarized SH radiation for a monolayer adsorbed onto a polymer-coated substrate in a similar manner, we find the expressions for $L_{xx}(2\omega)$ and $L_{zz}(2\omega)$ are also identical to the forms for the input field in Eq. (A3).

The output local-field factors for the cell geometry pictured in Fig. 9(b) are derived in a similar way, except that we do not have to worry about the field radiated in the positive z direction. Taking into account the transmission through each interface, we derive expressions that are identical in form to the input local-field factors of Eq. (A5) for the same system.

APPENDIX B: LOCAL-FIELD CORRECTIONS FOR OBLIQUELY EVAPORATED SiO_x SUBSTRATES

SHG from a clean, obliquely evaporated SiO_x surface shows an ansiotropic dependence on the sample rotation about the surface normal. The observed signal is pictured in Fig. 8(a). Since we know the SiO_x to be locally isotropic, we attribute the observed anisotropy to a geometrical effect. SEM pictures of obliquely evaporated SiO_x substrates indicate that the surface morphology is very complicated and, hence, difficult to model. Here, we present a qualitative model by assuming that the surface can be described by a sawtooth structure.

The sawtooth surface is modeled as a single wedge of angle $\eta=10°$ with the surface plane. To calculate the dependence of SHG on sample orientation, we must first transform the input fields from the laboratory frame (x,y,z) with $\hat{\mathbf{z}}$ along the surface normal and $\hat{\mathbf{y}}$ parallel to the grooves, to the local frame, (x',y',z'), with $\hat{\mathbf{z}}'$ along the wedge surface normal and $\hat{\mathbf{y}}'$ perpendicular to the $\mathbf{k}$-$\hat{\mathbf{z}}'$ plane where $\mathbf{k}$ is the wave vector [see Fig. 8(d)], calculate the SHG generated from the isotropic surface locally, and then transform the generated SH fields back to the laboratory frame. With the chosen local coordinates, the local plane of incidence lies in the $\hat{\mathbf{x}}'$-$\hat{\mathbf{z}}'$ plane. This allows us to use the same local-field factors defined in Eq. (A1) to calculate the SHG in the local frame. The Euler transformation from the laboratory frame to the local frame consists of three rotations,

$$\mathbf{R}=\mathbf{R}_3\mathbf{R}_2\mathbf{R}_1 ,$$

where

$$\mathbf{R}_1=\begin{bmatrix} \cos\Phi & \sin\Phi & 0 \\ -\sin\Phi & \cos\Phi & 0 \\ 0 & 0 & 1 \end{bmatrix},$$

$$\mathbf{R}_2=\begin{bmatrix} \cos\eta & 0 & \sin\eta \\ 0 & 1 & 0 \\ -\sin\eta & 0 & \cos\eta \end{bmatrix},$$

$$\mathbf{R}_3=\begin{bmatrix} \cos\psi & \sin\psi & 0 \\ -\sin\psi & \cos\psi & 0 \\ 0 & 0 & 1 \end{bmatrix}.$$

$\mathbf{R}_1$ corresponds to a rotation about the laboratory $\hat{\mathbf{z}}$ axis through an angle Φ, $\mathbf{R}_2$ is a rotation through the wedge angle η about the $\hat{\mathbf{y}}$ axis parallel to the grooves, and $\mathbf{R}_3$ is a rotation about ψ about the $\hat{\mathbf{z}}'$ axis to make the $\hat{\mathbf{x}}$-$\hat{\mathbf{z}}$ plane coincide with the local plane of incidence. We find, from the geometry,

$$\psi=\arctan\left[\frac{\sin\Phi\sin\theta_1}{\cos\eta\cos\Phi\sin\theta_1-\sin\eta\cos\theta_1}\right],$$

where θ_1 is the angle of incidence in the laboratory frame.

The effect of the wedge surface on the azimuthal dependence of SHG is twofold. First, it leads to a mixing of polarizations of a beam; i.e., a pure s or p input polarization in the laboratory frame will have both s and p components in the local frame. This mixing will depend on the sample orientation. The wedge also leads to a local angle of incidence that is dependent on sample orientation in the following way:

$$\theta_1'=\arccos(\cos\Phi\sin\eta\sin\theta_1+\cos\eta\cos\theta_1)$$

where θ_1' is the local angle of incidence. When calculating the SH fields in the local frame, we must use local-field factors as defined in Eq. (A1), with the local angle of incidence defined above. This leads to local-field factors that are dependent on sample orientation.

The results of the calculation are pictured next to the observed anisotropy in Fig. 8(c). As can be seen, the qualitative feature of the observed anisotropy is reproduced.

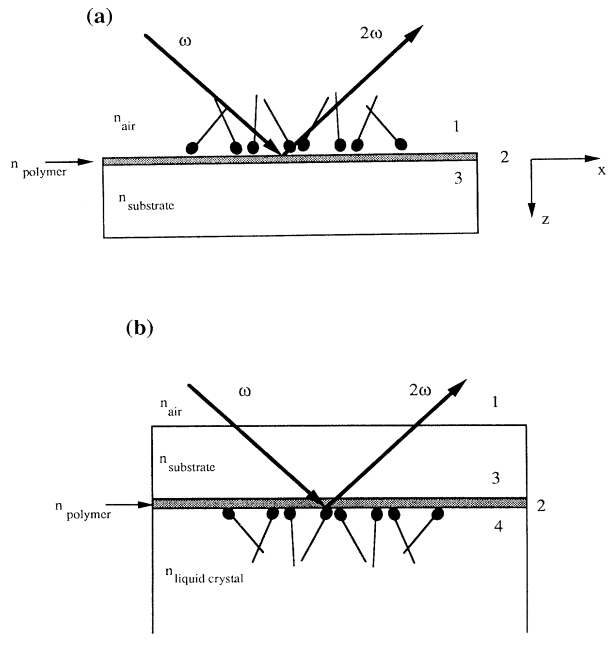

FIG. 9. Schematics for the interfaces used to calculate the local-field factors for an 8CB molecular monolayer adjacent to a polymer-coated substrate. (a) 8CB molecules are in air; (b) 8CB molecules are in contact with 8CB bulk.

*Present address: Greyhawk Systems Inc., Milpitas, CA 95035.
[1]See, for example, J. Cognard, Mol. Cryst. Liq. Cryst. **51**, 1 (1982).
[2]D. W. Berreman, Phys. Rev. Lett. **28**, 1683 (1972); Mol. Cryst. Liq. Cryst. **23**, 215 (1973).
[3]J. M. Geary, J. W. Goodby, A. R. Kmetz, and J. S. Patel, J. Appl. Phys. **62**, 4100 (1987).
[4]T. J. Sluckin and A. Poniewierski, in *Fluid Interfacial Phenomena,* edited by C. A. Croxton (Wiley, New York, 1986), Chap. 5, and references therein.
[5]W. Chen, L. J. Martinez-Miranda, H. Hsiung, and Y. R. Shen, Phys. Rev. Lett. **62**, 1860 (1989).
[6]K. Miyano, Phys. Rev. Lett. **43**, 51 (1979).
[7]H. Mada, J. Chem. Phys. **75**, 372 (1981).
[8]H. Yokoyama, Mol. Cryst. Liq. Cryst. **165**, 265 (1988).
[9]J. S. Foster and J. E. Frommer, Nature (London) **333**, 542 (1988); J. F. Spong, H. A. Mizes, L. J. Lacomb, M. M. Dovek, J. E. Frommer, and J. S. Foster, *ibid.* **338**, 137 (1989).
[10]W. Chen, M. B. Feller, and Y. R. Shen, Phys. Rev. Lett. **63**, 2665 (1989).
[11]G. Marowsky, G. Lupke, R. Steinhoff, L. F. Chi, and D. Mobius, Phys. Rev. B **41**, 4480 (1990).
[12]See, for example, Y. R. Shen, Annu. Rev. Phys. Chem. **40**, 327 (1989); Y. R. Shen, Nature (London) **337**, 519 (1989).
[13]G. Berkovic, Th. Rasing, and Y. R. Shen, J. Opt. Soc. Am. B **4**, 945 (1987).
[14]P. Guyot-Sionnest, H. Hsiung, and Y. R. Shen, Phys. Rev. Lett. **57**, 2963 (1986).
[15]P. Guyot-Sionnest and Y. R. Shen, Phys. Rev. B **38**, 7985 (1988).
[16]C. S. Mullin, P. Guyot-Sionnest, and Y. R. Shen, Phys. Rev. A **39**, 3745 (1989).
[17]T. Uchida, M. Hirano, and H. Sakai, Liq. Cryst. **5**, 1127 (1989).
[18]S. Kuniyosu, H. Fukuro, S. Maeda, K. Nakaya, M. Nmitta, N. Ozaki, and S. Kobayashi, Jpn. J. Appl. Phys. **27**, 827 (1988).
[19]S. Ishihara, H. Wakemoto, K. Nakazima, and Y. Matsuo, Liq. Cryst. **4**, 669 (1989).
[20]See, for example, P. G. deGennes, *The Physics of Liquid Crytals* (Clarendon, Oxford, 1974), p. 125.
[21]This is not generally true. With ferroelectric LC, the bulk alignment can deviate from the monolayer alignment. See W. Chen, Y. Ouchi, and Y. R. Shen (unpublished).
[22]F. J. Kahn, Appl. Phys. Lett. **22**, 386 (1973).
[23]J. L. Janning, Appl. Phys. Lett. **21**, 173 (1972).
[24]A. Rapini and M. Papoular, J. Phys. (Paris) Colloq. **30**, C4-54 (1969).
[25]G. Barbero, E. Miraldi, C. Oldano, M. L. Pastello, and P. T. Valabrega, J. Phys. (Paris) **47**, 1411 (1986).
[26]S. Naemura, J. Phys. (Paris) Colloq. **40**, C3-514 (1979).
[27]C. Rosenblatt, J. Phys. (Paris) **45**, 1987 (1984).
[28]S. Faetti, M. Gatti, V. Palleschi, and T. J. Sluckin, Phys. Rev. Lett. **55**, 1681 (1985); S. Faetti and V. Palleschi, Liq. Cryst. **2**, 261 (1987).
[29]H. Yokoyama, S. Kobayashi, and H. Kamei, J. Appl. Phys. **61**, 4501 (1987).
[30]T. Oh-Ide, S.Kuniyasu, and S. Kobayashi, Mol. Cryst. Liq. Cryst. **164**, 91 (1988).
[31]G. Barbero and S. Durand, Phys. Rev. A **41**, 2207 (1990).